Langmuir

Article

pubs.acs.org/Langmuir

Thermodynamics of Water Confined in Porous Calcium-Silicate-Hydrates

P. A. Bonnaud,[†] Q. Ji,[†,∥] B. Coasne,[§] R. J.-M. Pellenq,[‡,⊥] and K. J. Van Vliet*[,†]

[†]Department of Materials Science and Engineering and [‡]Department of Civil & Environmental Engineering, Massachusetts Institute of Technology, 77 Massachusetts Avenue, Cambridge, Massachusetts 02139-4307, United States

[∥]Inspur Group, State Key Laboratory of High-End Server & Storage Technology, Jinan, Shangdong, P. R. China

[§]Institut Charles Gerhardt Montpellier, CNRS UMR 5253, ENSCM, 8 rue de l'Ecole Normale, 34296 Montpellier Cedex 05, France

[⊥]Centre Interdisciplinaire de Nanoscience de Marseille, Aix-Marseille Université, UPR 3118 CNRS, Campus de Luminy − case 913, 13288 Marseille Cedex 9, France

ABSTRACT: Water within pores of cementitious materials plays a crucial role in the damage processes of cement pastes, particularly in the binding material comprising calcium-silicate-hydrates (C−S−H). Here, we employed Grand Canonical Monte Carlo simulations to investigate the properties of water confined at ambient temperature within and between C−S−H nanoparticles or "grains" as a function of the relative humidity (%RH). We address the effect of water on the cohesion of cement pastes by computing fluid internal pressures within and between grains as a function of %RH and intergranular separation distance, from 1 to 10 Å. We found that, within a C−S−H grain and between C−S−H grains, pores are completely filled with water for %RH larger than 20%. While the cohesion of the cement paste is mainly driven by the calcium ions in the C−S−H, water facilitates a disjoining behavior inside a C−S−H grain. Between C−S−H grains, confined water diminishes or enhances the cohesion of the material depending on the intergranular distance. At very low %RH, the loss of water increases the cohesion within a C−S−H grain and reduces the cohesion between C−S−H grains. These findings provide insights into the behavior of C−S−H in dry or high-temperature environments, with a loss of cohesion between C−S−H grains due to the loss of water content. Such quantification provides the necessary baseline to understand cement paste damaging upon extreme thermal, mechanical, and salt-rich environments.

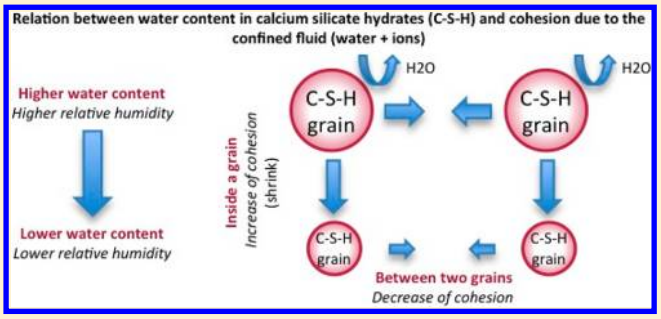

1. INTRODUCTION

Concrete, which is obtained by mixing cement, water, sand, and aggregates, is the most widely used engineering material in the world. In particular, this cementitious composite is exposed to a wide range of thermodynamic conditions (temperature, pressure, relative humidity, or presence of ions) that can reduce the durability of physical infrastructure. Key limitations to the sustainability of this ubiquitous material include resistance to weathering (freeze/thaw cycles), to chemical attack (sulfates, seawater, acid), to fire, and to high-rate mechanical loading. In most such damage processes, water confined within cement plays an important yet unclear role. In the classical picture of setting,[1] calcium-silicate-hydrates (or C−S−H with C = CaO; S = SiO_2; H = H_2O) comprise the binding phase that effectively glues together reaction products and nonreacting phases within the cement paste. This C−S−H phase exhibits multiscale porosity ranging from the nanometer to millimeter scales, such that water confined within the porous network of the material coexists in different states (gas, liquid, solid). Such phase coexistence and phase changes that occur upon varying the external conditions (e.g., in freeze/thaw cycles, fire, humidity) can result in significant structural and mechanical damage to cement pastes. Moreover, transport of corrosive species through the confined water phase also causes drastic damage to cementitious materials.

While reaching a clearer picture of the role of water confined within the smallest pores of the C−S−H phase is relevant to understanding damage evolution and aging of the material, this is a very challenging task from an experimental point of view. Approaches including the surface force apparatus,[2,3] atomic force microscopy,[4] nuclear magnetic resonance,[5] or quasi-elastic neutron scattering[6] provide access to many properties of water confined at the nanoscale. Nevertheless, the properties of confined water at the atomistic scale and their effect on pore structure remain to be clarified in the case of porous composites such as cement pastes. Atomistic simulations can aid in understanding such properties, as demonstrated in earlier works dealing with other porous materials such as amorphous and porous silica,[7] zeolites,[8,9] and clays.[10] For cementitious materials, simulations are suitable for understanding the growth mechanisms that govern the formation of the C−S−H phase,[11] the mechanical properties of a C−S−H monocrystal and

Received: April 27, 2012
Revised: June 25, 2012
Published: June 26, 2012

gels,[12,13] the origin and control of cohesion in cement,[14−16] and the cement nanotexture.[17] Some of these calculations have been validated by experiments, such as the prediction of the bulk modulus for tobermorite-like mineral phases.[18] Most of these simulations above have focused on the solid structure of C−S−H, with few exceptions[19,20] considering the role of confined water in the C−S−H structure and properties at various length scales and time scales. In this respect, Ji et al. conducted a benchmarking study[19] by considering different empirical atomistic force fields for water in order to gauge accurate prediction of the structural, mechanical, and dynamical properties of a single C−S−H grain. These authors found that both SPC-flexible[21] and TIP5P[22] water potentials were able to reproduce C−S−H experimental properties. Youssef et al.[20] explored the properties of water confined in the ultrasmall space available in a single C−S−H grain, and found that both interlayer calcium ions and defective silicate chains in the C−S−H structure contribute to the hydrophilic nature of C−S−H.

In these previous studies on a single C−S−H grain, the authors assumed that the nanoporosity of the grain is saturated with water (which corresponds to low temperature and/or high relative humidity or %RH). In reality, a C−S−H grain can be exposed to many different environmental conditions in terms of temperature and relative humidity RH = P/P_0 (where P is the pressure of the water vapor in the external environment, and P_0 the bulk saturating vapor pressure at the temperature T). Adsorption experiments (e.g., ref 23) are suitable for relating the water content and %RH at a given temperature. In contrast, to our knowledge, atomistic simulations have not been employed to estimate the adsorbed amount of water in a C−S−H grain (intragranular water content) as a function of the external relative humidity. Given that C−S−H can be considered as an assembly of grains,[24] one must also consider how the amount of water adsorbed in between the grains (an intergranular space of a few nm width) depends on the relative humidity. Youseff et al. showed clearly the hydrophilic nature of the intragranular C−S−H interfaces.[20] This implies that water forms a wetting film in contact with the C−S−H external surfaces and exerts a pressure between the grains which can be either positive or negative.[25,26] The latter is generally called the solvation pressure (or disjoining pressure)[27] and has been studied intensely over decades. (See ref 28 for a review.)

The aim of the present study is to employ atomistic simulations to study water confined at ambient temperature inside a C−S−H grain (intragranular) and between C−S−H grains (intergranular) for different relative humidities at 300 K. We also seek to understand how the solvation pressure evolves with water content, and how relative humidity affects the intragranular and intergranular cohesion due to the confined aqueous fluid in this material. We consider pores idealized as slits, with various widths up to 10 Å. Of course, the values considered are not representative of the entire porous network[23] but define the length scales over which cohesion among nanoscale C−S−H particles occurs. As discussed below, we quantify the C−S−H cohesion as a function of humidity and intergranular distance at 300 K, and then consider the behavior of C−S−H in environments characterized by very low %RH or elevated temperature.

2. METHODS

2.1. Atomistic Model for C−S−H Grains. Two atomistic models were designed (Figure 1). Here, note that the cement chemistry community denotes CaO as C, SiO_2 as S, and H_2O as H. Figure 1A shows the intragranular model describing a single C−S−H grain, and Figure 1B shows the intergranular model describing two C−S−H grains. The intragranular model is the defective C−S−H structure proposed by Pellenq et al.[17] The general chemical formula is $Ca_{99}Si_{60}O_{219}{\cdot}66H_2O$ at 100% RH in our work. The latter model has been used previously in atomistic simulations of water within C−S−H.[19,20] Two silicate-rich layers are explicitly described in the simulation box (L_1 and L_2 in Figure 1). The calcium-to-silicon ratio of this structure is C/S = 1.65, which is close to the mean value found using energy-dispersive X-ray analysis[29,30] of hardened Portland cement pastes aged from 1 day to 3.5 years (C/S = 1.70). Note that, in order to reach C/S = 1.65 in the model of C−S−H, Pellenq et al. removed hydroxyl groups from the original tobermorite structure.[17] However, the structural and mechanical properties predicted using this model show reasonable agreement with experiments.[17] The surface charge of this C−S−H structure is $\sigma = -0.73$ C.m^{-2}, which is 46% higher than the value for tobermorite (C/S = 1):[31] $\sigma = -0.5$ C.m^{-2}. The latter is a mineral considered analogous to C−S−H, although its C/S ratio differs from that of C−S−H. The charge in C−S−H is due to structural defects in the silica chains[17] and needs to be compensated by calcium counterions to keep the system electroneutral. The intragranular model is enclosed in a triclinic box of 13.31 × 29.52 × 23.69 Å^3 with the following angles: $\alpha = 92.02°$, $\beta = 88.52°$, and $\gamma = 123.58°$. The intergranular model is built up from the intragranular model that is used as a building unit. To do so, the intragranular cell is first duplicated along the x direction. Then, the two silicate-rich layers (L_1 and L_2 in Figure 1) are separated by a distance of H = 10 Å. Consequently, the intergranular model is enclosed in a triclinic box of 26.62 × 29.52 × 33.69 Å^3 with the following angles: $\alpha = 92.02°$, $\beta = 88.52°$, and $\gamma = 123.58°$.

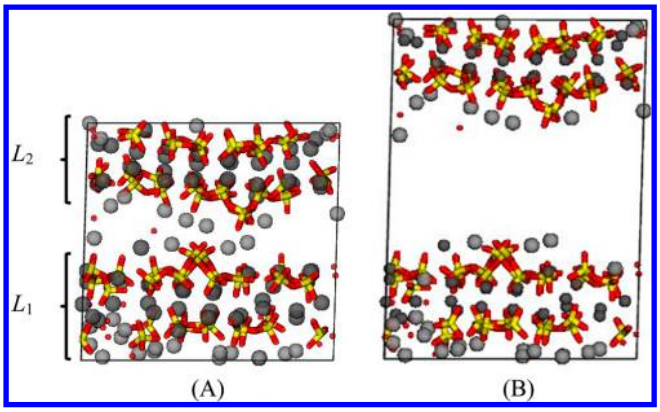

Figure 1. Simulation cells for calcium-silicate-hydrate (C−S−H), with water molecules removed for clarity. System (A), the monolithic structure or single grain, is the initial structure taken from ref 17. Two silicate-rich layers (L_1 and L_2) are explicitly described in this structure. System (B), the slit pore system, is constructed from (A): L_1 and L_2 are separated by a distance of H = 10 Å. The simulation box dimensions of system (A) and (B) are, respectively, 13.31 × 29.52 × 23.69 Å^3 and 26.62 × 29.52 × 33.69 Å^3 with the following angles: $\alpha = 92.02°$, $\beta = 88.52°$, and $\gamma = 123.58°$. Yellow and red segments are the bonds between Si and O atoms in the silica chains; dark gray spheres are for the calcium atoms belonging to the C−S−H layer; light gray spheres are for calcium counterions that compensate the negatively charged silica surface.

2.2. Intermolecular Potentials. Two types of interaction potentials are commonly used to simulate C−S−H materials: (i) core−shell potentials[32,33] and (ii) CLAYFF-like potentials.[34,35] In both cases, the short-range interactions which correspond to the dispersion−repulsion interactions are modeled using Lennard-Jones potentials (with parameters that are fitted to match some structural and physical properties).[36,37] In the core−shell model, atomic electronic polarizabilities are taken into account by representing atoms as a core and a massless shell.[38] Formal ionic charges are used for in-solid species[39] in order to make the core−shell interaction

dx.doi.org/10.1021/la301738p | Langmuir 2012, 28, 11422−11432

potential transferable.[35] In CLAYFF-like potentials, atomic partial charges are taken equal to the Mulliken charges,[40] which are determined using ab initio calculations.[35,37] In so doing, CLAYFF-like potentials are less transferable than core−shell potentials.

In the present work, we used a different approach. The derivation of partial charges is based on the ab initio simulation work of Shasavari et al.[35] First, the value for the partial charge of Si atoms is directly taken from the latter work, q_{Si} = +2.25e. Moreover, in the work of Shasavari et al., two partial charges for calcium ions are defined: + 1.66e for calcium ions that belong to the CaO layer in the C−S−H structure (intralayer ions) and +1.70e for interlayer calcium ions. In our work, we make the assumption that all the calcium ions have the same partial charge. Then, the mean value of those given by Shasavari et al. is considered, i.e., +1.68e. Finally, two partial charges are defined for oxygen atoms in the work of Shasavari et al. corresponding to oxygen atoms involved in an OH group (−1.22e) and to oxygen atoms involved in the silica chains of C−S−H (−1.36e). As in our C−S−H model, there is no hydroxyl group; we considered only the latter value. At that point, the sum of charges over the atoms of the C−S−H particle is not neutral in our model. Indeed, we find an excess of charge of +3.48e. In order to ensure the electroneutrality of the system, we adjust the oxygen charge to ∼ −1.376e. These charges are reported in Table 2. The main difference between our approach and the core−shell and CLAYFF-like potentials lies in the determination of the dispersion/repulsion part of the interactions between the fluid (water molecules and calcium counterions) and the C−S−H substrate. Indeed, instead of using Lennard-Jones potentials fitted to match structural and physical data, we used the mathematical form used in the PN-TrAZ model:[41]

$$U_{ij}(r_{ij}) = A_{ij}\exp(-b_{ij}r_{ij}) - \sum_{n=3}^{5} f_{2n}(r_{ij})\frac{C_{2n}^{ij}}{r_{ij}^{2n}} \quad (1)$$

where r_{ij} is the distance between an atom j of the silicate-rich layers (Si, O, or Ca in Table 2) and an atom i of the confined fluid (O_w, H_w, or C_w in Table 2). The first term in eq 1 is a Born-Mayer term corresponding to the short-range repulsive energy (repulsive interactions) that arises at short distance when the electron clouds of two atoms start to overlap. Parameters for the repulsive interactions between like-atoms are obtained with the help of *ab initio* quantum chemistry methods: parameters for Si, O, O_w, and H_w are taken from the work of Puibasset and Pellenq,[7] while parameters for calcium ions (Ca and C_w) are taken from the work of Owczarek et al.[42] The Böhm and Ahlrichs combination rules are used to describe cross-interactions between the different species.[43] Repulsive interaction parameters are given in Table 2. The second term in eq 1 is a multipolar expansion series of the dispersion interaction that can be obtained from the quantum mechanical perturbation theory applied to intermolecular forces.[44] Pellenq and Nicholson[41] have shown that two-body dispersion C_{2n}^{ij} coefficients for isolated or condensed-phase species can be derived from the dipole polarizability α and the effective number of polarizable electrons N_{eff} of all interacting species, which are closely related to partial charges that can be obtained from ab initio calculations. Polarizabilities for Si atoms and O atoms of the C−S−H structure, as well as O_w atoms and H_w atoms of the water molecules are taken from the work of Puibasset and Pellenq.[7] The polarizability for Ca and C_w ions is taken from the work of Pellenq and Nicholson.[41] α and N_{eff} are given for each species in Table 2. Note that f_{2n} in eq 1 is a damping function that depends on the distance r_{ij} and the repulsive parameter b_{ij}:

$$f_{2n}(r_{ij}) = 1 - \sum_{m=0}^{2n}\frac{(b_{ij}r_{ij})^m}{m!}\exp(-b_{ij}r_{ij}) \quad (2)$$

The use of the latter functions avoids the divergence of the dispersion interaction when the distance between two interacting species decreases down to the level of atomic diameters.[45] The PN-TrAZ procedure provides a means to derive the cross-parameters for each species with only partial charges, polarizabilities, and effective numbers of electrons as input data.[46] The cross-parameters are given in Table 3.

Table 1. Lennard-Jones Parameters for Atoms Comprising the Confined Fluid in Atomic Units (a_0 = 0.529 177 Å and 1 Ha = 4.359 744 × 10^{-8} J)[a]

species	σ [a_0]	$\varepsilon \times 10^{-4}$ [Ha]
O_w	5.98	2.4757
H_w	-	-
C_w	5.71	1.9867

[a]Lennard-Jones parameters for the calcium ions (C_w) are taken from ref 49. σ is the minimum distance between two atoms and ε is the well depth of the Lennard-Jones potential.

Table 2. Input Parameters in the PN-TrAZ Method[41] to Derive Dispersion and Repulsion Potential Parameters in Order to Describe Interactions between the Fluid and the Solid Species in the System (a_0 = 0.529 177 Å and 1 Ha = 4.359 744 × 10^{-8} J)[a]

	fluid species			C−S−H species		
label	C_w	O_w	H_w	Si	O	Ca
q [e]	+1.68	−0.82	+0.41	+2.25	−1.37589	+1.68
A [Ha]	990.7	247.7	1.338	6163.4	1543.5	990.7
b [a_0^{-1}]	2.374	2.075	2.11	2.395	2.19	2.374
α [a_0^3]	3.193	7.56	2.655	2.36	8.03	3.193
N_{eff}	6.106	4.476	0.414	1.279	5.032	6.106

[a]q is the partial charge of the atom, A and b are the repulsion parameters, α is the dipole polarizability, and N_{eff} is the effective number of electron of the atom.

Note that potentials derived with the PN-TrAZ procedure have previously shown good agreement with experiments for zeolites[47] and porous silica glass.[7]

For the description of the water molecules, we employed one of the most computationally efficient models, the rigid-SPC model[48] that does not take into account the flexibility of the water molecule. In doing so, we were able to simulate a large number of water molecules as encountered in our largest pores (N_{water} ∼360) in a reasonable amount of time. In the rigid-SPC potential, the angle between O_wH_w bonds of a water molecule is θ = 109.47° and the O_wH_w bond length is r_{OwHw} = 1 Å. The O_w and H_w atoms possess a partial charge that interacts through the Coulombic interaction. In addition, the O_w atom of the water molecule is a center of repulsion/dispersion interactions, which are described using a Lennard-Jones potential. Calcium counterions are also described as a Lennard-Jones sphere and a partial charge (+1.68e). In the latter case, Lennard-Jones parameters are taken from the work of Koneshan et al.[49] The Lorentz−Berthelot mixing rules are used to described cross-interactions between water and calcium counterions. For the fluid species, Lennard-Jones parameters are given in Table 1 and partial charges are given in Table 2. The cutoff radius to compute the dispersion/repulsion interactions is of R_{cut} = 6.5 Å for the intragranular model and R_{cut} = 12 Å for the intergranular model. The Coulomb energy was computed using the Ewald summation technique with the following parameters: κ = 0.27 $Å^{-1}$ for the intragranular model and κ = 0.24 $Å^{-1}$ for the intergranular model and a minimum of k_{max} = 5 for both systems (κ is the width of the Gaussian charge distribution surrounding each charge and k_{max} is the maximum number of k-vector in the reciprocal space in the direction corresponding to the smallest box dimension in the real space, $L = \|\vec{a}\|$, $\|\vec{b}\|$, or $\|\vec{c}\|$). The maximum k-vectors in the two other reciprocal space directions (k'_{max} and k''_{max}) are added or removed with respect to the real space length of the two other box dimensions (L' and L''): $k'_{max} = k_{max} \times L'/L$ and $k''_{max} \times L''/L$.

2.3. Grand Canonical Monte Carlo Technique. The water content within the C−S−H phase depends on the %RH in the external environment. To relate the water content, i.e., the quantity of adsorbed water, to a given %RH and a given temperature T = 300 K we computed adsorption isotherms. To do so, we employed the Grand

dx.doi.org/10.1021/la301738p | Langmuir 2012, 28, 11422−11432

Table 3. Repulsion and Dispersion Parameters Obtained Following the PN-TrAZ Method[46a]

fluid species	C−S−H Species	C_6 [Ha.a_0^6]	C_8 [Ha.a_0^8]	C_{10} [Ha.a_0^{10}]	A [Ha]	b [a_0^{-1}]
H_w	O	8.4253	133.4797	4167.9202	45.4445	2.1493
H_w	Si	2.4156	31.445	964.788	90.8109	2.2435
H_w	Ca	3.906	75.5199	2210.7227	36.4076	2.2344
O_w	O	35.5305	603.071	20553.6465	618.3243	2.1309
O_w	Si	10.0686	145.3636	4673.8324	1235.5866	2.2235
O_w	Ca	17.9006	343.0666	11191.4996	495.3671	2.2146
C_w	O	19.3615	260.6015	5650.2785	1236.5666	2.2785
C_w	Si	5.4303	60.5450	985.9659	2471.0092	2.3847
C_w	Ca	10.5740	157.3314	1636.8537	990.6686	2.3744

[a]Böhm and Ahlrichs combination rules[43] are used to determine the repulsive parameters between unlike species, including an atom that is within the aqueous electrolyte (subscript w) and in the solid (no subscript).

Canonical Monte Carlo technique (GCMC). In such a technique, the volume V of the system (the intra- or intergranular model of C−S−H with the adsorbed phase) is constant and is in equilibrium with an infinite reservoir of water molecules imposing its chemical potential μ and temperature T.[50] To define RH = P/P_0, the pressure P of the gas reservoir of water molecules is deduced from the chemical potential according to the bulk equation of state for an ideal gas. The saturating vapor pressure of the rigid-SPC water model is P_0 = 4.4 kPa.[51] Only the number of water molecules was allowed to fluctuate in the simulation box as the calcium counterions were treated in the canonical ensemble: each ion was allowed to move, while the number of ions remained constant. As these ions compensate the surface charge of the silicate-rich layers, this ensures that the system remains electroneutral. To reduce computing time, the silicate-rich layers were kept fixed in the course of the simulation. Then the adsorbate/substrate interactions were computed using an energy grid. The potential energy is calculated at each corner of each triclinic element (about 0.2 × 0.2 × 0.2 Å^3 with the following angles: α = 92.02°, β = 88.52°, and γ = 123.58°). In the course of the simulation, the grid values were interpolated in a linear fashion to provide an accurate estimate of the energy. Such a procedure has been shown[52] to simulate adsorption in mesoporous media of complex morphology and/or topology without a direct summation over matrix species during the GCMC runs. Periodic boundary conditions were used along the x, y, and z directions. Finally, simulations for each data point in this work were performed in two sequential procedures. First, GCMC equilibration runs of at least 100 million accepted steps were performed to reach system equilibria (stable energy (fluctuations around a mean value) and stable exchange of water molecules (number of inserted water molecules ≈ number of removed water molecules). Data were then obtained using a GCMC production run of 200 million accepted steps with a sampling of atomic configurations every 10 000 accepted steps.

2.4. Calculation of Intra- And Intergranular Pressures. To provide insight regarding the intra- and intergranular cohesion, we computed the internal fluid pressure. Indeed, this approach has been employed previously to capture cohesion in structureless models of C−S−H grains[14] and in atomistically described models of muscovite mica sheets.[53] In our study, we are interested in the internal fluid pressure that is transmitted to the C−S−H structure, i.e., the pressure (P_N) that is applied in the direction normal to the silicate-rich layers of our models (pore surface). Using the virial expression[50] of the pressure, which consists of correcting the perfect gas law, we can write the normal pressure as

$$P_N = P_{Ideal} + P_{FF} + P_{FS} \tag{3}$$

where $P_{Ideal} = \rho k_B T$ is the ideal pressure predicted by the perfect gas law, ρ being the number density, k_B the Boltzmann constant, and T the temperature. P_{FF} and P_{FS} are, respectively, the pressure contribution arising from interactions among the fluid molecules

$$P_{FF} = \frac{1}{V}\sum_{i=1}^{N_{fluid}}\sum_{j>i}^{N_{fluid}} \vec{f}_{ij,z}^{\,FF}\cdot\vec{z}_{ij} \tag{4}$$

and the pressure contribution arising from interactions between the fluid molecules and the solid C−S−H substrate

$$P_{FS} = \frac{1}{V}\sum_{i=1}^{N_{fluid}}\sum_{j=1}^{N_{solid}} \vec{f}_{ij,z}^{\,FS}\cdot\vec{z}_{ij} \tag{5}$$

where N_{fluid} is the number of fluid molecules, N_{solid} the number of solid atoms, V the volume of the fluid (water molecules and calcium ions), and z_{ij} the z-component of the distance between an atom i and an atom j. $\vec{f}_{ij,z}^{\,FF} = \vec{f}_{ij,z}^{\,LJ} + \vec{f}_{ij,z}^{\,Ew}$ and $\vec{f}_{ij,z}^{\,FS} = \vec{f}_{ij,z}^{\,PN} + \vec{f}_{ij,z}^{\,Ew}$ are, respectively, the force exerted by an atom j of the fluid on an atom i of the fluid and the force exerted by an atom j of the solid on an atom i of the fluid. Furthermore, the mathematical description of Lennard-Jones forces, $\vec{f}_{ij,z}^{\,LJ}$, and Ewald forces, $\vec{f}_{ij,z}^{\,Ew}$, can be, respectively, found in refs 53 and 54. For the PN-TrAZ forces, we used the following form:

$$\vec{f}_{ij,z}^{\,PN} = \left[A_{ij}b_{ij}\exp(-b_{ij}r_{ij}) - \sum_{n=3}^{5} 2n\,\frac{C_{2n}^{ij}}{r_{ij}^{2n+1}}\,g_{2n}(r_{ij})\right]\frac{\vec{z}_{ij}}{r_{ij}} \tag{6}$$

where

$$g_{2n}(r_{ij}) = 1 - \sum_{m=0}^{2n}\left(1 + \frac{b_{ij}r_{ij} - m}{2n}\right)\frac{(b_{ij}r_{ij})^m}{m!}\exp(-b_{ij}r_{ij}) \tag{7}$$

In our approach, the confined fluid comprises two components: the water molecules and the calcium counterions. This assumption is the same as that of Gmira et al.,[14] but departs from the work of Malani et al.,[53] which considered only water as part of the fluid. The present approach enables better understanding of the origin of the cohesion in the C−S−H phase. In this study, we computed the pressure inside the fluid, which means that a negative pressure indicates a cohesive behavior and a positive pressure indicates a disjoining or repulsive behavior between pore faces. Finally, the way we share the pressure in a fluid−fluid contribution (P_{FF}) and in a fluid−solid contribution (P_{FS}) is not the only option. Indeed, it is also possible to compute for each species of the fluid (water molecules (H_2O) and calcium ions (C_w)) the pressure contribution that arises from dispersion-repulsion interactions ($P_{Disp-Rep}$) and the pressure contribution that arises from electrostatic interactions (P_{Ewald}). In our work, $P_{Disp-Rep}$ is always positive and P_{Ewald} is always negative. Moreover, they are usually on the same order of magnitude, which is around 1 to 10 GPa. As the ideal part of the pressure is 1 to 2 orders of magnitude lower than these two latter contributions, the normal pressure P_N is mainly driven by the balance between $P_{Disp-Rep}$ and P_{Ewald}. In order to quantify this, we compute the ratio $|P_{disp-rep}|/|P_{Ewald}|$. When the ratio is greater than 1, $P_{Disp-Rep}$ contributes mainly to P_N. When the ratio is lower than 1, P_{Ewald} contributes mainly to P_N. Results for the intragranular and intergranular models are summarized in Table 4. We observe that inside the grain dispersion/repulsion interactions for water play a major role in the normal pressure. The reverse situation is observed between the grains where the normal pressure is mainly driven by the electrostatic interactions. For calcium ions, whatever the location,

dx.doi.org/10.1021/la301738p | Langmuir 2012, 28, 11422−11432

Table 4. Ratio $|P_{disp-rep}|/|P_{Ewald}|$ for Each of the Fluid Species: Water Molecules (H_2O) and Calcium Ions (C_w)[a]

model	location	species	$\lvert P_{disp-rep}\rvert/\lvert P_{Ewald}\rvert$
intragranular	inside the grain	H_2O	1.36
		C_w	0.64
intergranular	inside the grain	H_2O	2.67
		C_w	0.70
	between the grains	H_2O	0.90
		C_w	0.52

[a] $P_{Disp-Rep}$ is the pressure contribution that arises from dispersion-repulsion interactions and P_{Ewald} is the pressure contribution that arises from electrostatic interactions. Results are given for the intragranular and the intergranular models. Note that, when the ratio is greater than 1, $P_{Disp-Rep}$ contributes mainly to the normal pressure (P_N), and when the ratio is lower than 1, P_{Ewald} contributes mainly to P_N.

electrostatic interactions always contribute significantly to the normal pressure.

3. RESULTS AND DISCUSSION

3.1. How Does Relative Humidity Affect Water Content? Water content is a key factor in C−S−H, as this parameter can change both the physical and thermodynamic properties of the water that, in turn, affect C−S−H properties. In order to relate the water content to the relative humidity in the external environment for the intragranular and the intergranular models, we computed adsorption isotherms at 300 K (Figure 2). Figure 2a compares the adsorption isotherm for the same atomic intragranular model using both CSHFF[35] (a CLAYFF-like potential) and the PN-TRAZ potentials. The adsorption isotherm shapes are in fair agreement; the PN-TRAZ potential used for the remainder of this study predicts a more hydrophilic behavior. Thus, the C−S−H grain contains more water and has a higher density (2.21 g.cm^{-3}) than that obtained using the CSHFF potential (2.18 g.cm^{-3}). This agreement is not as good as that obtained previously with the more computationally expensive core−shell potential,[17] but still remains in fair agreement with the experimental density[31] at ambient pressure and temperature (2.6 g.cm^{-3}). Figure 3 shows typical molecular configurations for water adsorbed at different relative humidities in the intragranular and intergranular C−S−H models, so that the filling of the pores can be visualized.

In the intragranular model, the adsorption isotherm shows a continuous and reversible pore filling with a large number of adsorbed water molecules at small relative humidities. Indeed, the C−S−H grain is nearly filled with water around 1% RH, which further demonstrates that C−S−H is a highly hydrophilic material. Considering the intergranular model, we observe that the adsorption mechanism is different than for the intragranular model. As in the case of a single C−S−H grain, there is a large number of water molecules adsorbed at low relative humidity, underscoring the hydrophilicity. However, due to the presence of the intergrain space of pore width H = 10 Å, the complete pore filling appears at higher RH than what is observed in the intraganular model. Note the formation of a water bridge beyond 4% RH (see Figure 3b), that grows in thickness (in a similar way as for the adsorbed water layer on the grain surface) up to 14% RH (before capillary condensation). This is due to surface roughness of our grain model that acts, for such narrow pores, as constrictions promoting liquid water formation. This bridging is expected, based on earlier work by Coasne and Pellenq for adsorption of

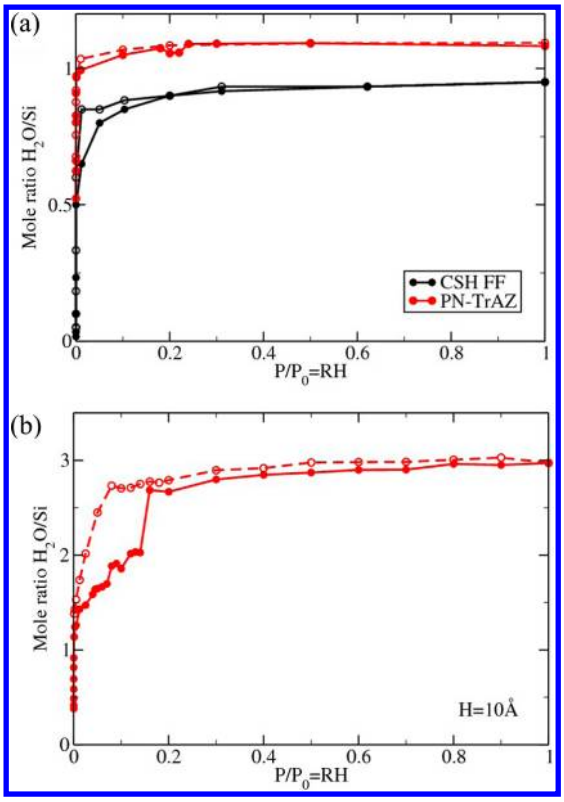

Figure 2. Adsorption (filled symbols) and desorption (empty symbols) isotherms of water in different calcium−silicate−hydrate (C−S−H) systems: (a) in the monolithic structure (system A) representing a single C−S−H grain, and (b) in a slit pore of width H = 10 Å between two C−S−H grains (system B). Red circles represent data obtained in this work with the PN-TrAZ potential; black circles represent data with the CSH-FF potential.

simple fluids in porous silica (e.g., refs 52 and 55). Moreover, a discontinuity is observed in the adsorption path at ∼15% RH. This is due to capillary condensation, i.e., sudden pore filling (see Figure 3c). Immediately following capillary condensation, the fluid in the core of the pore is not completely saturated compared to the bulk value. This is why a small increase in water content is observed even after capillary condensation has occurred, in order to recover the bulk fluid density in the core of the pore. The desorption in our intergranular model is continuous, and departs from the adsorption path. As was stated in a previous simulation study of water adsorption in amorphous silica slit pores,[56] desorption in our model (an infinite slit pore) is affected by the fact that the fluid cannot evaporate via the displacement of a hemicylindrical meniscus. Desorption in slit pore systems usually appears via a one-step process (cavitation) when there is a hysteresis in the isotherm. However, in our simulations of desorption in C−S−H slit pores, we do not observe such a discontinuity. This difference is due to the high surface roughness in our system relative to the pore width (see Figure 1) that hinders the usual desorption mechanism. Finally, in the intra- and intergranular models, we observed that above 20% RH all nanometer-scale cement pores are filled with water. This atomistic picture of confined water is in agreement with the colloidal model detailed by Jennings et al.,[57] which included globules each comprising an assembly of building blocks (our C−S−H grains) with a radius of 28 Å that were full of water at 20% RH.

dx.doi.org/10.1021/la301738p | Langmuir 2012, 28, 11422−11432

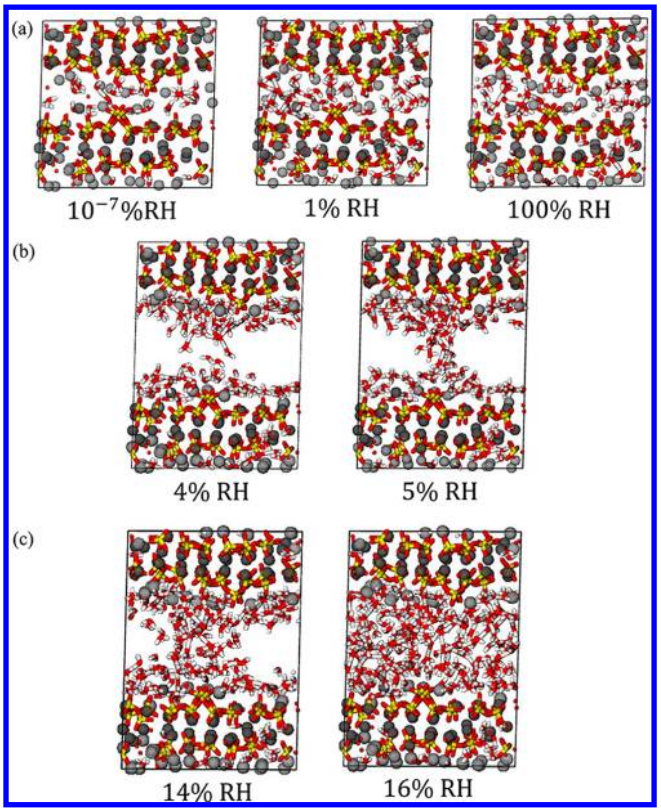

Figure 3. (a) Snapshots of pore filling at T = 300 K in the single calcium−silicate−hydrate (C−S−H) grain (system A, intragranular). Three relative humidities are considered (RH = P/P_0, P being the pressure of the gas reservoir of water molecules that is in contact with the system and P_0 being the saturating vapor pressure of the rigid-SPC water model): 10^{-7}%, 1%, and 100%. Due to the nanoporosity, the system is nearly filled with water molecules at 1% RH. For pore filling in the slit pore of C−S−H of a width H = 10 Å (system B, intergranular), two situations are considered: (b) before (4%RH) and after (5%RH) the water bridge formation, and (c) before (14%RH) and after (16%RH) the capillary condensation.

The adsorption process is an exothermic process. In order to quantify the heat released during adsorption, we computed the isosteric heat of adsorption (Q_{ST}), which is the opposite value of the differential enthalpy of adsorption. It is obtained from cross fluctuations over the total potential energy U and water-adsorbed amount N

$$Q_{ST} = RT - \frac{\partial U}{\partial N} = -\Delta H_{ads} \quad (8)$$

where R is the ideal gas constant and T is the temperature. Q_{ST} as a function of the relative humidity for the intra- and intergranular models is reported and compared to experiments in Figure 4. Experiments were performed on tobermorite, the crystalline mineral structure related closely to C−S−H, at ∼274 K.[58] In the latter case, even if the temperature is lower than in our simulations (300 K), previous experiments can help us to understand water behavior in this material. Indeed, previous simulations on Vycor (porous silica glass)[7] showed that an increase of the temperature from 300 to 350 K does not affect significantly Q_{ST} values at low adsorbed amount (low RH), but decreases Q_{ST} by 8% as large amounts of water are adsorbed. We then expect that, similarly to porous silica, if the experiment were performed at 300 K instead of 274 K, few changes will be observed at low adsorbed amount and an increase of Q_{ST} at

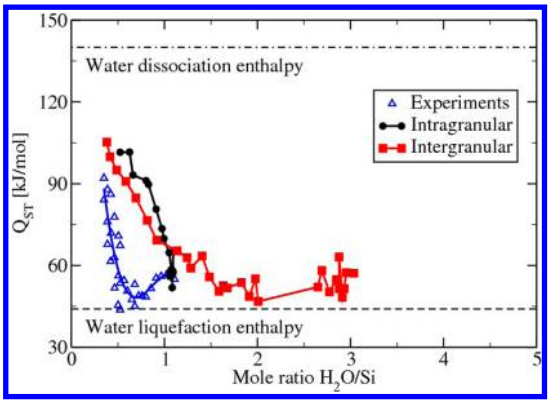

Figure 4. Isosteric heat of adsorption of water in the single calcium−silicate−hydrate (C−S−H) grain (system A) [black filled circles] and in the slit pore of C−S−H of a width H = 10 Å (system B) [red filled squares]. Black dashed line represents the experimental value of the water liquefaction enthalpy; black dashed−dotted line represents the experimental value of the water dissociation enthalpy. Results are compared with experiments (blue triangles) for tobermorite (C/S = 1).[58]

large adsorbed amounts. For both models in our simulations, Q_{ST} values at low adsorbed amounts tend to values around 120 kJ.mol^{-1}, which is three times the water liquefaction enthalpy. This means that at the first stage of the adsorption process, water molecules preferentially interact with the surface (adsorption) rather than with the other water molecules inside the pore volume. In other words, and as was stated previously in our analysis of adsorption isotherms, both our intergranular and intragranular C−S−H models are highly hydrophilic. Moreover, the values that we found are in relatively good agreement with experiments on tobermorite minerals (C/S = 1). The higher values found in our simulations may partly be explained by the relatively higher C/S ratio in our model. The latter makes C−S−H in our model more hydrophilic due to the affinity between calcium and water. When the water-adsorbed quantity increases, Q_{ST} values for both models decrease. This behavior is a clear indication that surfaces in our models are energetically heterogeneous.

Note that, in the intragranular model of C−S−H, which is a defective model of crystalline tobermorite, Q_{ST} approaches ∼55 kJ.mol^{-1} but does not decrease down to the water liquefaction enthalpy. This limiting value at high water content is in fair agreement with experiments.[58] However, we note that, in contrast to our findings for C−S−H, Q_{ST} reaches this enthalpy as a local minimum for tobermorite. This difference may be due to (i) the highly defective nature of C−S−H, as compared to crystalline tobermorite, (ii) the difference in C/S ratio, or (iii) an oversimplification of our C−S−H computational model (e.g., rigid silicate-rich layers and rigid water model). Finally, one of the advantages of computing Q_{ST} is that integration over the relative humidity gives the quantity of heat needed to dry the sample,[59,60] which is in our case the C−S−H phase. These heat quantities are of particular interest in the scope of understanding cement durability in a dry environment or at high temperatures, preceding heat-induced polymerization of silica chains. Results for the intra- and intergranular models give, respectively, ∼61 kJ.mol^{-1} and ∼55 kJ.mol^{-1}. A lower value for the intergranular model is expected, given the fact that there is a larger space between the grains. Water confined in this space is energetically less costly to remove than water confined within a single, nanoscale C−S−H grain.

dx.doi.org/10.1021/la301738p | Langmuir 2012, 28, 11422−11432

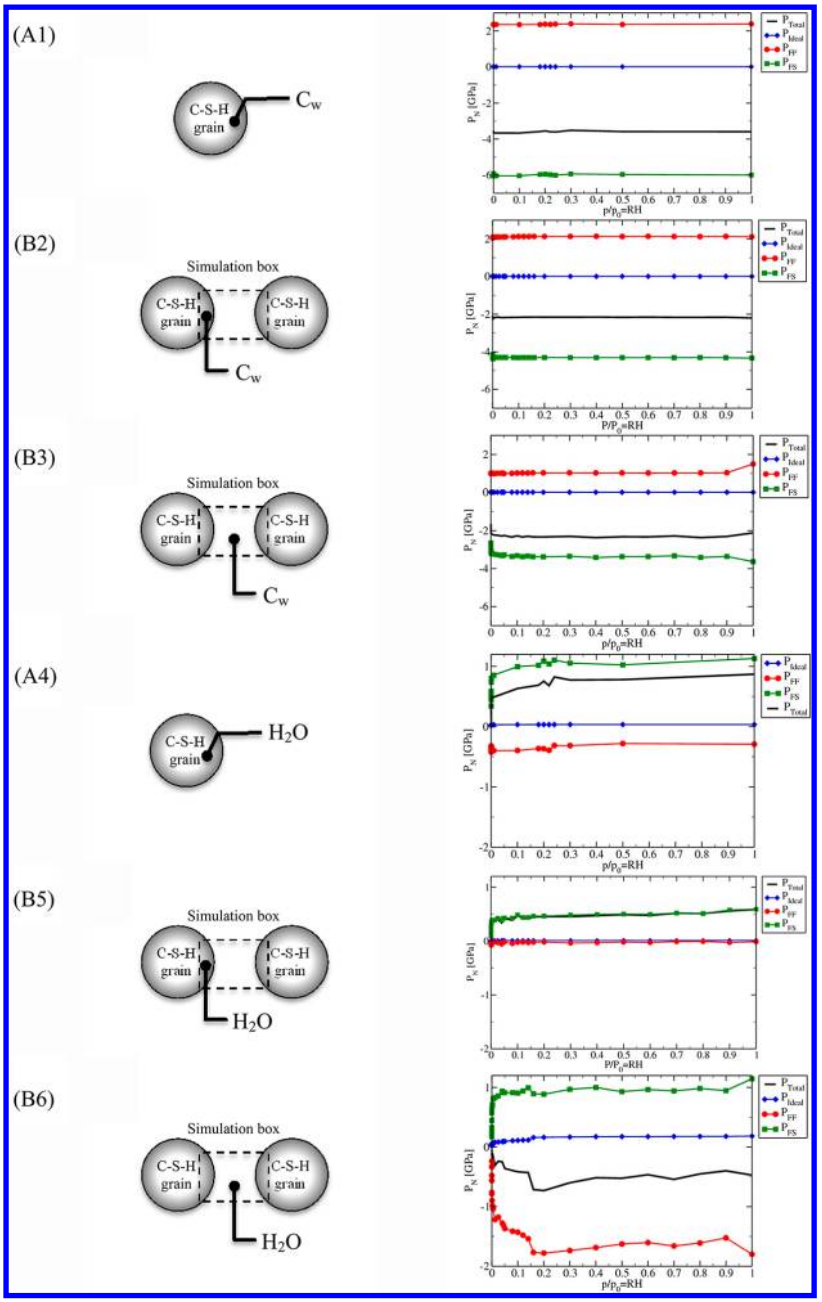

Figure 5. Isotherm of pressure for water (H_2O) and calcium (C_w) ions in the single calcium−silicate−hydrate (C−S−H) grain (system A) and in the slit pore of C−S−H of a width H = 10 Å (system B). In the first column of the figure, pictograms represent the location of the species for which the pressure has been computed. A connector ended by a black filled circle is used to represent the location of the species on the pictogram. When the black filled circle is located inside the gray disk that represents the C−S−H grain, it means that pressure is computed inside the grain. When the black filled circle is located outside the gray disks, it means that pressure is computed between the grains. The second column gives the total pressures (thick black lines) resulting from the presence of confined C_w ions ((A1), (B2), and (B3)) or confined water ((A4), (B5), and (B6)) inside the grain or between the grains. The second column also gives the different contributions to the total pressure: (i) the ideal pressure predicted by the perfect gas law (blue filled diamonds); (ii) the absolute value of the pressure contribution arising from the interaction among the fluid molecules (red filled circles); and (iii) the absolute value of the pressure contribution arising from the interaction between the fluid molecules and the solid C−S−H substrate (green filled squares).

3.2. How Does the Relative Humidity Affect Intra- And Intergranular Cohesion? To assess the effect of water content on the cohesion in our models, we computed the fluid internal pressure for different RH (Figure 5). Contributions of the calcium counterions to the pressure are given in (A1) for the intragranular model and in (B2) and (B3) for the intergranular model. In all cases under study, we observed a nearly constant and highly negative pressure coming from the calcium counterions. The latter fact provides clear evidence that calcium counterions are responsible for the cohesion due to the fluid inside the grain and between the grains. Furthermore, considering the different contributions to the pressure, we observed that these high negative pressures are mainly driven by interactions with the substrate (silicate-rich layers). Contributions of the water molecules to the pressure are given in (A4), (B5), and (B6). We observed that the behavior

dx.doi.org/10.1021/la301738p | *Langmuir* 2012, 28, 11422−11432

of water is different between two grains (B6) compared to the situation inside a grain ((A4) and (B5)). Indeed, in the former case, pressures due to water are negative and then contribute to the cohesion between the grains. Moreover, prior to capillary condensation when RH increases, pressures decrease so that cohesion increases. Upon capillary condensation (15%RH), there is a pressure drop as was observed in a previous theoretical study on simple fluids in micropores.[27] Above capillary condensation, the pressure rises slowly as the density of confined water molecules reaches the bulk density. Thereafter, increasing the water content (or RH) increases the cohesion between the grains. Considering these different contributions, we find clearly that the cohesive behavior originates from the fluid−fluid interactions, whereas the fluid−substrate interactions contribute a disjoining behavior. Inside the grain ((A4) and (B5)), water exhibits an overall disjoining behavior (positive pressures) that increases with RH. In that case, reducing RH (or water content) increases the cohesion in the grain. For example, if we let the structure relax it would shrink. The latter assumption is confirmed by experiments by Cong and Kirkpatrick, in which a decrease of the basal spacing (space between the silicate-rich layers) was observed upon drying,[61] i.e., a decrease of %RH. That experiment also validates our approach that does not account explicitly for chemical reactions, because those authors found that the polymerization of C−S−H was not affected in the range 9% < RH < 100% at ambient temperature. However, a more disordered local structure was observed upon decrease of RH.

Considering the total internal fluid pressure (i.e., the sum of contributions from water and calcium counterions) in the intra- and intergranular models, we observed that up to about 20% RH the overall cohesion is affected by the change in the water content (Figure 6). As we stated above, inside a C−S−H grain,

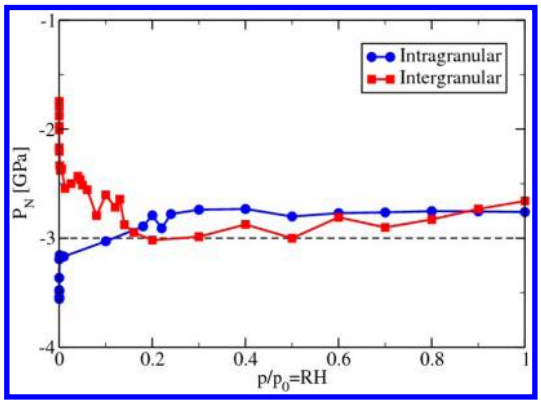

Figure 6. Isotherms of the total internal fluid pressure (i.e., the sum of contributions from water and calcium counterions) for the intra- (blue filled circles) and intergranular (red filled squares) models of calcium−silicate−hydrate (C−S−H). Our results are compared to the value of the computed rupture strength (dashed black line) of C−S−H obtained in ref 17.

the cohesion is decreased (grains swell due to water that has a disjoining behavior) and cohesion among C−S−H grains is increased. Thus, the overall cohesion due to the fluid of an assembly of these C−S−H grains will increase with increasing %RH. Moreover, above 20% RH, beyond which all nanometer-scale cement pores are filled with water, the overall cohesion inside a C−S−H grain is relatively stable ($P_N \approx 2.75$ GPa), which is in fair agreement with a previous simulation result in which the rupture strength of the same C−S−H structure was evaluated (∼3 GPa).[17] In the intergranular model, we observed that cohesion between C−S−H grains is relatively stable ($P_N \approx 3$ GPa) in the range 20% < RH < 50% prior to decrease beyond 50% RH. On one hand, these results help to explain the reduced strength of concrete in very dry environments (RH < 20%), and provide insight toward damage mechanisms in concrete at high temperatures (e.g., fire environments) even prior to heat-induced polymerization of silica chains.[61] Indeed, these conditions lead to a loss of water content in C−S−H paste.[61] If water content is lower than the level of ∼2.6 H_2O/Si, i.e., 20% RH at 300 K, then cohesion will be reduced among C−S−H grains. On the other hand, these results help to explain the creep behavior of cement at higher water content. Jennings et al. well summarized the latter phenomenon in a recent paper,[62] noting that creep rates decreased with decreasing relative humidity and were particularly low for less than 50% RH. Our results show that cohesion due to the confined fluid is reinforced by about 13% down to 50% RH. Thus, movement between C−S−H grains, which serve as the basic building block of the globules as described in that colloidal model,[57] is more hindered at 50% RH. Although cement paste is clearly multiscaled, this role of water at the nanometer-scale provides one length scale of explanation for creep reduction at low relative humidity.

3.3. How Should We Account for Multiscaled Porosity of Cement? The above discussion considered two configurations: one that mimics the situation inside a grain, and another that mimics the situation in which two grains are separated by a distance of H = 10 Å. We considered only one pore size, though C−S−H exhibits multiscale porosity. To consider the effects of pore size, Figure 7 summarizes computations for which the distance between the C−S−H grains was varied from H = 0 to 10 Å with a distance step of 1 Å. First, the pressure difference that can be observed between H = 0 Å and H = 1 Å is not physical, but is due to geometrical considerations. Indeed, at H = 0 Å, when the two grains are in contact (similar to a single grain view), we consider the intergranular model. Now, at H = 1 Å, a space is created between the two silicate-rich layers (intergranular model). Then, as we compute the different pressure contributions (inside the grain and between the grains), some differences appear compared to the intragranular model due to the geometric criteria we used to divide the space in our intergranular model. Note also that in Figure 7 we considered the situation for grains at 100% RH, i.e., where effects of the fluid are the strongest. The first information that we have from these computations is that the distance separating a grain from another grain does not affect the fluid inside the grain. Indeed, considering the top frame of Figure 7, we note that the fluid pressure inside the grain is nearly constant with respect to the intergranular distance and exhibits a cohesive behavior. Considering the contributions coming from each species within the fluid, it is clear that this pressure is mainly driven by the contribution of calcium counterions, as the pressure from water is constant and positive (disjoining behavior). Considering the internal fluid pressure between the grains (bottom of Figure 7), we observe strong cohesive behavior at short distances ($P_N \approx -20$ GPa for H = 1 Å) that decreases in intensity, as H increases ($P_N \approx -3$ GPa for H = 10 Å). Moreover, we found again that the behavior of the total internal pressure is mainly driven by calcium counterions. Interestingly, the behavior of

dx.doi.org/10.1021/la301738p | Langmuir 2012, 28, 11422−11432

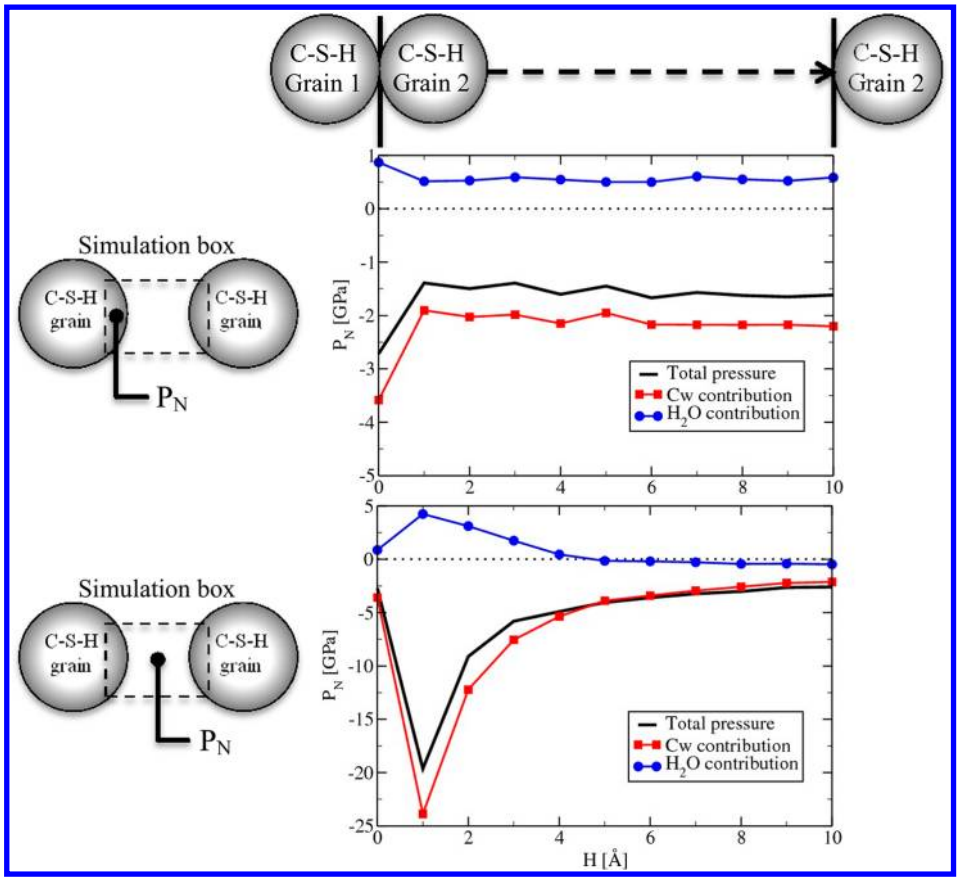

Figure 7. Total pressure (thick black line), contribution of the calcium (C_w) ions to the pressure (red squares), and contribution of water (H_2O) to the pressure (blue circles) as a function of the distance between the calcium−silicate−hydrate (C−S−H) grain C−S−H grains. As shown in the graphics, the top figure represents the pressure of the fluid (water and C_w ions) confined within the grain, and the bottom figure represents the pressure of the fluid (water and C_w ions) confined between the grains.

water is changed at the intergranular distance of 5 Å. Below separations of 5 Å, the water pressure is positive and, as a consequence, reduces the cohesion. Above separations of 5 Å, the pressure of water is negative and increases the cohesion.

4. SUMMARY AND OUTLOOK

In summary, we employed numerical simulations to provide a clearer understanding of the thermodynamics of water confined within the smallest pore sizes of C−S−H, the binding phase of cement. This picture is relevant in our scientific approach to understand and to improve the durability of cement by understanding damage mechanisms. Employing a new approach to describe interactions between the fluid and the C−S−H substrate, we addressed three fundamental questions:

How does the relative humidity affect water content? Adsorption isotherms were computed to relate the water content in the C−S−H porosities and the relative humidity of the environment. We found that, up to porosities of width H = 10 Å, pores are completely filled with water down to relative humidity of 20%. We then computed isosteric heat of adsorption that gave the energy released upon water adsorption in C−S−H. The latter quantity, which also indicates how much heat is required to dry the system, is relevant to understanding C−S−H behavior at high temperatures or in dry environments.

How does the relative humidity affect intra- and intergranular cohesion? We computed the fluid internal pressure (water molecules and calcium counterions) for different relative humidities. We found that, inside the grain and between grains, pressures were highly negative and thus indicated a cohesive behavior. We also found that this cohesion originates chiefly from the calcium counterions that interact strongly with the C−S−H substrate. Contribution of water molecules within the confined fluid lead to a disjoining behavior inside the C−S−H grain and a cohesive behavior between the C−S−H grains.

How should we account for multiscaled porosity of cement? We computed the fluid internal pressure for different intergranular distances. We highlight the fact that there is no effect of this distance on the cohesion due to the fluid confined inside a grain. Between the C−S−H grains, the fluid also contributes to cohesion that is driven chiefly by calcium counterions. Depending on the intergranular distance, the presence of water molecules may reduce (<5 Å) or increase (>5 Å) the cohesion.

Finally, these findings suggest the first idea of C−S−H behavior in dry or high temperature environments, with a loss of cohesion between the C−S−H grains due to the loss of water content. Because of the assumptions imposed to construct our models, it is obviously not possible to accurately highlight C−S−H cohesion behavior for temperatures that are sufficiently high to induce silica polymerization. Such effects of the confined fluid on cohesion at low temperatures or in high-pressure environments are areas of future work that can now build upon this baseline of water thermodynamics under ambient conditions.

dx.doi.org/10.1021/la301738p | *Langmuir* 2012, 28, 11422−11432

AUTHOR INFORMATION

Corresponding Author

*E-mail: krystyn@mit.edu.

Notes

The authors declare no competing financial interest.

ACKNOWLEDGMENTS

This work was sponsored by the U.S. Department of Homeland Security, Science and Technology Directorate, Infrastructure Protection and Disaster Management Division: Ms. Mila Kennett, Program Manager. The research was performed under the direction of Dr. Beverly P. DiPaolo, Engineer Research and Development Center (ERDC), U.S. Army Corps of Engineers. We acknowledge funding from the MIT Concrete Sustainability Hub, supported by the Portland Cement Association (PCA) and Ready Mix Concrete (RMC) Research & Education Foundation. We acknowledge the MIT-France foundation (MIT Seed-Fund) for funding part of this work. Finally, we acknowledge the CINaM-CNRS laboratory for access to computational facilities.

REFERENCES

(1) Vernet, C.; Cadoret, G. Les BHP, caractéristiques, durabilité, applications; Presses de l'ENPC: Paris, 1992; pp 115−128.

(2) Cottin-Bizonne, C.; Steinberger, A.; Cross, B.; Raccurt, O.; Charlaix, E. Nanohydrodynamics: The Intrinsic Flow Boundary Condition on Smooth Surfaces. *Langmuir* **2008**, *24*, 1165.

(3) Israelachvili, J.; Pashley, R. The hydrophobic interaction is long range, decaying exponentially with distance. *Nature* **1982**, *300*, 341.

(4) Plassard, C.; Lesniewska, E.; Pochard, I.; Nonat, A. Nanoscale Experimental Investigation of Particle Interactions at the Origin of the Cohesion of Cement. *Langmuir* **2005**, *21*, 7263.

(5) Levitz, P.; Korb, J.-P.; Petit, D. Slow dynamics of embedded fluid in mesoscopic confining systems as probed by NMR relaxometry. *Eur. Phys. J. E* **2003**, *12*, 29.

(6) Bordallo, H.; Aldridge, L. Concrete and Cement Paste Studied by Quasi- Elastic Neutron Scattering. *Z. Phys. Chem.* **2010**, *224*, 183.

(7) Puibasset, J.; Pellenq, R. J.-M. A grand canonical Monte Carlo simulation study of water adsorption on Vycor-like hydrophilic mesoporous silica at different temperatures. *J. Phys.: Condens. Matter* **2004**, *16*, S5329.

(8) Desbiens, N.; Boutin, A.; Demachy, I. Water Condensation in Hydrophobic Silicalite-1 Zeolite: A Molecular Simulation Study. *J. Phys. Chem. B* **2005**, *109*, 24071.

(9) Abrioux, C.; Coasne, B.; Maurin, G.; Henn, F.; Jeffroy, M.; Boutin, A. Cation Behavior in Faujasite Zeolites upon Water Adsorption: A Combination of Monte Carlo and Molecular Dynamics Simulations. *J. Phys. Chem. C* **2009**, *113*, 10696.

(10) Rotenberg, B.; Marry, V.; Vuilleumier, R.; Malikova, N.; Simon, C.; Turq, P. Water and ions in clays: Unraveling the interlayer/micropore exchange using molecular dynamics. *Geochim. Cosmochim. Acta* **2007**, *71*, 5089.

(11) Manzano, H.; Ayuela, A.; Dolado, J. S. On the formation of cementitious C−S−H nanoparticles. *J. Comput.-Aided Mater. Des.* **2007**, *14*, 45.

(12) Manzano, H.; Dolado, J. S.; Guerrero, A.; Ayuela, A. Mechanical properties of crystalline calcium-silicate-hydrates: comparison with cementitious C-S-H gels. *Phys. Stat. Solidi A* **2007**, *204* (6), 1775.

(13) Shahsavari, R.; Buehler, M. J.; Pellenq, R. J.-M.; Ulm, F.-J. First-Principles Study of Elastic Constants and Interlayer Interactions of Complex Hydrated Oxides: Case Study of Tobermorite and Jennite. *J. Am. Ceram. Soc.* **2009**, *92* (10), 2323.

(14) Gmira, A.; Zabat, M.; Pellenq, R. J.-M.; Van Damme, H. Microscopic physical basis of the poromechanical behavior of cement-based materials. *Materials Structures/Concrete Science and Engineering* **2004**, *37*, 3.

(15) Pellenq, R. J.-M.; Lequeux, N.; Van Damme, H. Engineering the bonding scheme in C−S−H: The iono-covalent framework. *Cem. Concr. Res.* **2008**, *38*, 159.

(16) Jönsson, B.; Nonat, A.; Labbez, C.; Cabane, B.; Wennerström, H. Controlling the Cohesion of Cement Paste. *Langmuir* **2005**, *21*, 9211.

(17) Pellenq, R. J.-M.; Kushima, A.; Shahsavari, R.; Van Vliet, K. J.; Buehler, M. J.; Yip, S.; Ulm, F.-J. A realistic molecular model of cement hydrates. *Proc. Natl. Acad. Sci. U. S. A.* **2009**, *106* (38), 16102.

(18) Oh, J. E.; Clark, S. M.; Monteiro, P. J. M. Does the Al substitution in C−S−H(I) change its mechanical property? *Cement and Concrete Research* **2011**, *41*, 102.

(19) Ji, Q.; Pellenq, R. J.-M.; Van Vliet, K. J. Comparison of computational water models for simulation of calcium−silicate−hydrate. *Comput. Mater. Sci.* **2012**, *53*, 234.

(20) Youssef, M.; Pellenq, R. J.-M.; Yildiz, B. Glassy Nature of Water in an Ultraconfining Disordered Material: The Case of Calcium-Silicate-Hydrate. *J. Am. Chem. Soc.* **2011**, *133*, 2499.

(21) Teleman, O.; Jönsson, B.; Engström, S. A Molecular-Dynamics Simulation of a Water Model with Intramolecular Degrees of Freedom. *Mol. Phys.* **1987**, *60*, 193.

(22) Mahoney, M. W.; Jorgensen, W. L. A five-site model for liquid water and the reproduction of the density anomaly by rigid, nonpolarizable potential functions. *J. Chem. Phys.* **2000**, *112* (20), 8910.

(23) Ranaivomanana, H.; Verdier, J.; Sellier, A.; Bourbon, X. Toward a better comprehension and modeling of hysteresis cycles in the water sorption−desorption process for cement based materials. *Cem. Concr. Res.* **2011**, *41*, 817.

(24) Constantinides, G.; Ulm, F.-J. The nanogranular nature of C−S−H. *J. Mech. Phys. Solids* **2007**, *55*, 64.

(25) Long, Y.; Palmer, J. C.; Coasne, B.; Sliwinska-Bartkowiak, M.; Gubbins, K. E. Pressure enhancement in carbon nanopores: a major confinement effect. *Phys. Chem. Chem. Phys.* **2011**, *13*, 17163.

(26) Long, Y.; Palmer, J. C.; Coasne, B.; Sliwinska-Bartkowiak, M.; Gubbins, K. E. Under pressure: Quasi-high pressure effects in nanopores. *Microporous Mesoporous Mater.* **2012**, *154*, 19.

(27) Balbuena, P. B.; Berry, D.; Gubbins, K. E. Theoretical Interpretation of Adsorption Behavior of Simple Fluids in Slit Pores. *J. Phys. Chem.* **1993**, *97* (4), 937.

(28) Derjaguin, B. V.; Rabinovich, Y. I.; Churaev, N. V. Direct Measurement of Molecular Forces. *Nature* **1978**, *272*, 313.

(29) Groves, G. W.; Le Sueur, P. J.; Sinclair, W. Transmission Electron Microscopy and Microanalytical Studies of Ion-Beam-Thinned Sections of Tricalcium Silicate Paste. *J. Am. Ceram. Soc.* **1986**, *69*, 353.

(30) Richardson, I. G.; Groves, G. W. Microstructure and microanalysis of hardened cement pastes involving ground granulated blast-furnace slag. *J. Mater. Sci.* **1992**, *27*, 6204.

(31) Allen, A. J.; Thomas, J. J.; Jennings, H. M. Composition and density of nanoscale calcium−silicate−hydrate in cement. *Nat. Mater.* **2007**, *6*, 311.

(32) Du, Z.; de Leeuw, N. H. A combined density functional theory□and interatomic potential-based simulation study of the hydration of nano-particulate silicate surfaces. *Surf. Sci.* **2004**, *554*, 193.

(33) Puertas, F.; Palacios, M.; Manzano, H; Dolado, J. S.; Rico, A.; Rodríguez, J. A model for the C-A-S-H gel formed in alkali-activated slag cements. *J. Eur. Ceram. Soc.* **2011**, *31*, 2043.

(34) Kalinichev, A. G.; Kirkpatrick, R. J. Molecular Dynamics Modeling of Chloride Binding to the Surfaces of Calcium Hydroxide, Hydrated Calcium Aluminate, and Calcium Silicate Phases. *Chem. Mater.* **2002**, *14*, 3349.

(35) Shahsavari, R.; Pellenq, R. J.-M.; Ulm, F.-J. Empirical force fields for complex hydrated calcio-silicate layered materials. *Phys. Chem. Chem. Phys.* **2011**, *13*, 1002.

(36) Catlow, C. R. A.; Thomas, J. M.; Parker, S. C.; Jefferson, D. A. Simulating Silicate Structures and the structural chemistry of pyroxenoids. *Nature* **1982**, *295*, 658.

(37) Cygan, R. T.; Liang, J.-J.; Kalinichev, A. G. Molecular Models of Hydroxide, Oxyhydroxide, and Clay Phases and the Development of a General Force Field. *J. Phys. Chem. B* **2004**, *108* (4), 1255.
(38) de Leeuw, N. H.; Higgins, F. M.; Parker, S. C. Modeling the Surface Structure and Stability of α-Quartz. *J. Phys. Chem. B* **1999**, *103*, 1270.
(39) Sanders, M. J.; Leslie, M.; Catlow, C. R. A. Interatomic Potentials for SiO_2. *J. Chem. Soc., Chem. Comm.* **1984**, 1271.
(40) Mulliken, R. S. Electronic Population Analysis on LCAO-MO Molecular Wave Functions.* I. *J. Chem. Phys.* **1955**, *23* (10), 1833.
(41) Pellenq, R. J.-M.; Nicholson, D. Intermolecular Potential Function for the Physical Adsorption of Rare Gases in Silicalite. *J. Phys. Chem.* **1994**, *98*, 13339.
(42) Owczarek, E.; Hawlicka, E. Molecular Dynamics Study of $CaCl_2$ in Methanol. *J. Phys. Chem. B* **2006**, *110* (45), 22712.
(43) Böhm, H.-J.; Ahlrichs, R. A study of short-range repulsions. *J. Chem. Phys.* **1982**, *77* (4), 2028.
(44) Stone, A. *The Theory of Intermolecular Forces*; Clarendon: Oxford, 1996.
(45) Tang, K. T.; Toennies, J. P. An improved simple model for the van der Waals potential based on universal damping functions for the dispersion coefficients. *J. Chem. Phys.* **1984**, *80*, 3726.
(46) Pellenq, R. J.-M.; Nicholson, D. A simple method for calculating dispersion coefficients for isolated and condensed-phase species. *Mol. Phys.* **1998**, *95* (3), 549.
(47) Puibasset, J.; Pellenq, R. J.-M. Grand Canonical Monte Carlo Simulation Study of Water Adsorption in Silicalite at 300 K. *J. Phys. Chem. B* **2008**, *112*, 6390.
(48) Berendsen, H. J. C.; Postma, J. P. M.; Van Gunsteren, W. F.; Hermans, J. Interaction Models for Water in Relation to Protein Hydration, in *Intermolecular Forces*, Pullman, B., Ed.; Reidel: Dordrecht, 1981; p 331.
(49) Koneshan, S.; Rasaiah, J. C.; Lynden-Bell, R. M.; Lee, S. H. Solvent Structure, Dynamics, and Ion Mobility in Aqueous Solutions at 25°C. *J. Phys. Chem. B* **1998**, *102*, 4193.
(50) Frenkel, D.; Smit, B. *Understanding Molecular Simulation: From Algorithms to Applications*, 2nd ed.; Academic Press: London, 2002.
(51) Vorholz, J.; Harismiadis, V. I.; Rumpf, B.; Panagiotopoulos, A. Z.; Maurer, G. Vapor + liquid equilibrium of water, carbon dioxide, and the binary system, water carbon dioxide, from molecular simulation. *Fluid Phase Equilib.* **2000**, *170*, 203.
(52) Coasne, B.; Pellenq, R. J.-M. A grand canonical Monte Carlo study of capillary condensation in mesoporous media: Effect of the pore morphology and topology. *J. Chem. Phys.* **2004**, *121* (8), 3767.
(53) Malani, A.; Ayappa, K. G.; Murad, S. Influence of Hydrophilic Surface Specificity on the Structural Properties of Confined Water. *J. Phys. Chem. B* **2009**, *113* (42), 13825.
(54) Deserno, M.; Holm, C. How to mesh up Ewald sums. I. A theoretical and numerical comparison of various particle mesh routines. *J. Chem. Phys.* **1998**, *109* (18), 7678.
(55) Coasne, B.; Pellenq, R. J.-M. Grand canonical Monte Carlo simulation of argon adsorption at the surface of silica nanopores: Effect of pore size, pore morphology, and surface roughness. *J. Chem. Phys.* **2004**, *120* (6), 2913.
(56) Bonnaud, P. A.; Coasne, B.; Pellenq, R. J.-M. Molecular simulation of water confined in nanoporous silica. *J. Phys.: Condens. Matter* **2010**, *22*, 284110.
(57) Jennings, H. M. Colloid model of C-S-H and implications to the problem of creep and shrinkage. *Materials and Structures* **2004**, *37*, 59.
(58) Costalin, L.; Van Damme, H. Thermodynamique de l'adsorption d'eau dans la tobermorite, une étude expérimentale; Internal Communication; Centre de Recherche sur la Matière Divisée, Centre National de la Recherche Scientifique, UMR 6619 (Université Orléans).
(59) Berlier, K.; Frère, M. Adsorption of CO_2 on Activated Carbon: Simultaneous Determination of Integral Heat and Isotherm of Adsorption. *J. Chem. Eng. Data* **1996**, *41*, 1144.
(60) Ferradji, A.; Malek, A. Isothermes d'Adsorption des Abricots Secs à 25°C et 45°C. *Rev. Energ. Ren.* **2005**, *8*, 39.
(61) Cong, X.; Kirkpatrick, J. Effect of the temperature and relative humidity on the structure of C-S-H gel. *Cem. Concr. Res.* **1995**, *25* (6), 1237.
(62) Jennings, H. M.; Bullard, J. W.; Thomas, J. J.; Andrade, J. E.; Chen, J. J.; Scherer, G. W. Characterization and modeling of pores and surfaces in cement paste: correlations to processing and properties. *Journal of Advanced Concrete Technology* **2008**, *6* (1), 5.